Enhancing air filtration efficiency with triboelectric nanogenerators in face masks and industrial filters

Nano Energy 112 (2023) 108514

Contents lists available at ScienceDirect

Nano Energy

journal homepage: www.elsevier.com/locate/nanoen

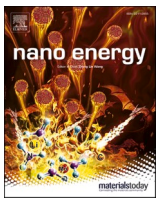

Enhancing air filtration efficiency with triboelectric nanogenerators in face masks and industrial filters

Masoumeh Karimi Kisomi [a], Sadegh Seddighi [a,b,*], Raheleh Mohammadpour [c], Alireza Rezaniakolaei [d]

[a] Department of Mechanical Engineering, K. N. Toosi University of Technology, Iran
[b] Division of Energy Technology, Chalmers University of Technology, Gothenburg, Sweden
[c] Institute for Nanoscience and Nanotechnology, Sharif University of Technology, Iran
[d] Department of AAU Energy, Aalborg University, Aalborg, Denmark

ARTICLE INFO

Keywords:
Triboelectric nanogenerator
Smart face mask
Electrostatic
Industrial air filter
Self-powered
Human health

ABSTRACT

The removal efficiency of traditional air filters decreases with decreasing particle size, requiring the use of highly compact filter layers to achieve high efficiency, resulting in high-pressure drops and power consumption. To address this issue, this study proposes a novel approach by combining triboelectric nanogenerator (TENG) properties with industrial air filters and face masks to improve removal efficiency while maintaining low-pressure drop. The study investigates the impacts of key parameters, such as airflow velocity, particle size, and applied voltage, on filter performance through a developed mathematical model. The optimal voltage range required to remove specific particle sizes is also modeled, and suitable triboelectric materials for producing the optimal voltage are suggested. Results show that the use of the suggested triboelectric-based filter, generated using a polypropylene (PP)-polyurethane (PU) TENG pair, with a 300 μm filter thickness, 30 μm pore size, and 30 μm fiber diameter, enhances the removal efficiency of particles from 23.0 % to 99.0 %. Specifically, a 10 V voltage on the fiber surface enables the removal of particles in the range of 10 nm to 100 μm with an efficiency of 99.0 %, which is 4 times higher than a traditional filter. The study demonstrates the potential of utilizing various antibacterial and polymer-based triboelectric materials in different applications, including self-powered smart face masks and industrial air filters.

1. Introduction

Air pollution and particulate matter (PM) have made negative impacts on human health such as cardiovascular and respiratory diseases [1,2]. Thus, it is necessary to promote efficient methods for the removal of PM to reduce the negative health impacts of particles. Various technologies have been used for air filtration, such as melt-blown polymers, metal-organic framework-based membranes, and electrostatic precipitators [3–5]. Among different methods, electrostatic attraction (EA) is widely used due to its superior capacity in binding and clinging nanoparticles to fibers. The electrostatic precipitator (ESP) is the method used to collect particles from the air stream using a charger electrode and a collector electrode. In this method, particles are charged by a charger electrode and subjected to electric forces leading to particle absorption on a collector electrode [1,6].

In recent years, several studies have been conducted on ESP. Zhang et al. [7] numerically studied the impacts of electric potential field, particle charge-to-mass ratio, solid volume fraction, fiber diameter, and face velocity on filtration performance. According to their results, decreasing fiber diameter and increasing particle size improved filtration efficiency. Also, increasing the velocity decreased efficiency. As well, when the solid volume fraction increased the removal efficiency increased but the pressure drop and solid volume fraction had a linear relationship, so but pressure drop increased. Lee et al. [8] investigated the effects of electrostatic and structural characteristics of filters on the removal efficiency and pressure drop. Based on their study, the particles were captured by coulomb force. Furthermore, the filter thickness had little influence on removal efficiency, but the efficiency was affected by the extent of inter-fiber distance and the fiber packing density. By increasing the number of sheets, the efficiency increased but the quality factor decreased because of the increase in the pressure drop. Long et al. [9] evaluated the efficiency and power consumption of a pleated filter.

* Corresponding author at: Division of Energy Technology, Chalmers University of Technology, Gothenburg, Sweden.
E-mail address: sadeghsk@kth.se (S. Seddighi).

https://doi.org/10.1016/j.nanoen.2023.108514
Received 3 March 2023; Received in revised form 4 May 2023; Accepted 8 May 2023
Available online 9 May 2023

They investigated the parameter's effects such as the corona discharge, airflow, wire position, plate height, and distance between plates on the filtration performance. Their results showed that shorter distances, lengthier plates, and lower airflow velocity resulted in increased efficiency. Also, the higher applied voltage increased the removal efficiency but it made the power consumption increase.

Generally, increasing pack density or applying a higher voltage can increase filtration efficiency, leading to a higher pressure drop and power consumption. And although electrostatic precipitators can be effective for air purification, they can be harmful to human health because of ozone production [10]. To solve this issue, the triboelectric effect is used to charge fibers [9]. The triboelectric nanogenerator consists of two materials with different affinities that could produce voltage and current by moving relative to each other [11]. TENG mechanism is based on the triboelectrification phenomenon and electrostatic induction. In triboelectrification, contact between two electrodes makes a charge and by separation from each other, the electrons flow between two electrodes by electrostatic induction phenomenon [12–14]. The application of TENG technology in filters presents a noteworthy advantage, as it results in increased filtration efficiency without any increase in pressure drop, power consumption, or ozone production. Furthermore, the mass or density of the structure remains constant and maintains high air permeability [3,15,16]. Another advantage is that TENG systems can employ low-frequency vibration in the environment to produce power such as the natural vibration of moving air in the channel or the car's tailpipe and also biomechanical energy such as breathing and speaking [3,17–19]. Also, TENG material has properties such as flexibility and antibacterial effect that is helpful for human health [20,21]. Furthermore, the TENG materials' compatibility with the human body has been proven that used in a wide range of technology such as self-powered tactile sensing and breathable electronic skin [16,19]. Some studies investigated employing TENG in air filtration. Wang et al. [22] studied air cleaning based on a multi-layered R-TENG. Their design consisted of a rotator and a stator that was driven by wind power to remove sulfur dioxide (SO_2) and dust. In their experimental setup, the R-TENG was connected to the two copper meshes as anode and cathode plates. Based on the electrochemical reaction, SO_2 lost two electrons and change to sulfuric acid so adsorbed on the anode copper mesh and removed from the air. Jeong et al. [23] fabricated a flexible porous structure film in combination with metal nanoparticles with a high dielectric constant. In their study, the dielectric film absorbed dust particles into the pore by triboelectric properties. They analyzed the collection efficiency of PM_{10} and $PM_{2.5}$. According to their results, the flexible film had 20.0 % higher efficiency than a film without metal nanoparticles. Kim et al. [24] designed a new structure by using a 3D printing method. Their design had a high surface area in comparing flat structures and was used for the dust-adsorption ($PM_{2.5}$) system. According to their study, the designed TENG had a removal efficiency of about 40.0 %. In recent years, several studies have been conducted on utilizing triboelectric technology in the face mask. Wang et al. [2] developed a self-powered face mask based on nanofiber electrospun that was enhanced by a TENG. They reached a removal efficiency of 86.0 % for ultrafine particles ($PM_{0.1}$). Zhou et al. [25] developed an electrospun polyetherimide (PEI) electret nonwoven face mask that can be used for healthcare monitoring and particulate matter removal. The removal efficiency was about 99.0 % for sub-micron NaCl particles (0.3 μm). In the study of Lustig et al. [26] various masks were investigated under steady-state, forced convection air flux with pulsed aerosols that simulate forceful respiration. Finally, the effective designs were noted. Wang et al.[27] fabricated a multilayered antibacterial nanofiber air filter that was enhanced by the TENG and had an average removal efficiency of 89.9 % for $PM_{0.1}$. Rajib et al. [28] focused on virus-laden aerosols and designed a smart mask by using a TENG. In their study, the viruses were killed by electrocuting through the electric field of TENG. Wang et al. [4] preferred a five-layer washable mask based on TENG that had a removal efficiency of about and 96.0 % for $PM_{2.5}$, but the removal efficiency decreased to 85.0 % for $PM_{0.5}$.

Recent research has shown that the effectiveness of various filtration technologies differs significantly for different particle sizes. Filtration of nano-sized particles is particularly challenging, as these particles can easily pass through the openings between fibers, thereby reducing the removal efficiency of the filter. To achieve high removal efficiency for such particles, a high packing density is required, which increases the pressure drop across the filter. Consequently, developing a technology that can enhance the PM collection efficiency and maintain filter performance without increasing the pressure drop remains a challenge. To address the challenge of decreasing removal efficiency for small-sized particles, the triboelectric nanogenerator is being explored to improve the removal efficiency of filters. While larger particles can be removed through mechanical means, small particles can be charged via the triboelectric effect and then separated from the air using electrostatic force. A TENG-based filtration model can thus maintain filter performance for small particles while avoiding pressure and removal efficiency drops.

This study focuses on the optimization of the voltage in the filtration system for enhancing the removal efficiency of particles within a specific range of sizes. To this end, the triboelectric nanogenerator is incorporated in the filtration system to supply the required voltage, and the optimal triboelectric material is selected for the filter design. The integration of triboelectric effects in conventional filtration materials allows for improved removal efficiency without the need for changes in the structure, pressure drops, or costs. A key contribution of this work is the prediction of the optimal voltage required for achieving high particle removal efficiency in a gas-particle multiphase flow. The resulting filters have potential applications in self-charged face masks and industrial filters, with the selection of the appropriate material for each filter design.

This paper aims to enhance the efficiency of face masks and industrial filters by utilizing triboelectric nanogenerator technology. The study investigates the effect of various operational parameters, such as airflow velocities, applied voltages, and particle diameters, on the removal efficiency of particles. The unique challenge of addressing a wide range of human breath velocity and particle motion in industrial channels, in addition to the diverse virus and dust particle sizes, is addressed in this work. To achieve this goal, a TENG module is numerically simulated using governing equations of TENG, two-phase flow, and electrostatic effect on particles. The study seeks to predict the optimal voltage range, identify suitable triboelectric materials for TENG filtration, study the impact of particle size on removal efficiency, and investigate the effect of airflow velocity on filtration efficiency. The findings demonstrate the promising potential of TENG-based filtration for various applications, offering a practical solution to the negative impacts of air pollution and particulate matter on human health. The study's novelty lies in the comprehensive analysis of the effect of various parameters on the efficiency of TENG-based filters, offering insight into optimizing their design and enhancing their performance. This work provides an advantage in that the TENG filtration efficiency is provided for a wide range of materials and particle sizes. The wide range of particle sizes studied in this work is an asset for designing new filters' to obtain the best filtration efficiency using various materials which consequently produce their associated TENG voltage separating especial particles.

2. Modeling

2.1. Governing equation

This work presents a numerical method for simulating multiphase flow using the discrete element method for particle motion and the finite element method for fluid flow. The Euler-Lagrangian method is employed for simulating two-phase flow, with particle trajectory in a Lagrangian frame of reference and airflow in an Eulerian frame of

reference. External forces such as electrostatic, drag, and Brownian forces affect particle motion in the fluid flow. In this study, the Laplace equation is used to solve the electrostatic forces and TENG model according to Gauss's law, while Navier-Stokes equations and Newton's law are used to solve fluid flow and particle motion, respectively. The resulting two-dimensional model is used to construct fiber structure, particle trajectory, and the associated airflow around fibers. A 2D symmetry model is used for the simulation of particle motion in a fluid flow. The 2D simulation of the particle motion in the flow of the filter application is also used by previous studies such as [8], [6], and [29]. The model enables the prediction of removal efficiency and pressure drop under different parameters such as air velocity, electric potential, and particle diameter. With this model, it is possible to determine the required voltage within a certain range of particle diameter and velocity to achieve the desired separation. Additionally, the model facilitates the identification of the triboelectric material capable of providing the necessary voltage.

2.1.1. Airflow

In this study, the Reynolds number is low (less than 2000) and the flow is considered to be laminar. The continuity equation and Navier-Strokes equations are solved for the airflow field in the steady state condition as follows [30]:

$$\frac{\partial \rho}{\partial t} + \frac{\partial u_j}{\partial x_j} = 0 \tag{1}$$

$$\frac{\partial \rho u_i}{\partial t} + \frac{\partial u_i u_j}{\partial x_j} = \frac{\partial P}{\partial x_i} + \frac{\partial}{\partial x_j}\left(\mu\left(\frac{\partial u_i}{\partial x_j} + \frac{\partial u_j}{\partial x_i} - \frac{2}{3}\delta_{ij}\frac{\partial u_k}{x_k}\right)\right) \tag{2}$$

Where u(m/s) is velocity, ρ(kg/m^3) is density, P(pa) is pressure,$\delta(-)$*is* the Kronecker delta and μ(Pa.s) is the viscosity of the continuous flow. In most industrial applications, the airflow is turbulent which affects the particles' motion. Therefore, it is important to choose the best turbulence model that matches the study. In this study, based on the Reynolds number, the K-ε model is used which is suitable for the high Reynolds [31] number range. Also, based on the studies presented in [32] and [33], the K-ε model is recommended in turbulence airflow in industrial application simulations such as duct and HVAC. To resolve the flow in the near-wall region, the two-layer model in combination with enhanced wall functions is used for the wall treatment. The combination of the two-layer model with enhanced wall functions is recommended in references [34,35] for the simulation of particle deposition.

2.1.2. Particles trajectory

Particles are captured by fiber filtration based on five mechanisms: gravity sedimentation, inertial impaction, interception, diffusion, and electrostatic interaction [7,28,36]. The behavior of a suspended particle in the fluid flow is described by Stokes number that is related to particle diameters, fluid velocity, and particle relaxation time [30,37]. The studies have shown that large particles (larger than 1 μm) are affected by gravitational force, but medium-sized particles (1–10 μm) are affected by sedimentation and impaction mechanism. In small-sized, (100 nm-11 μm), particles get diffused by mechanical interception and Brownian motion [28,38,39].

The trajectory of a particle is calculated by solving the net forces on the particle. The acting forces are the sum of the drag force, electrostatic force, Brownian force, virtual mass, thermophoretic force, and gravity force. While the drag force is proportional to the fluid viscosity, the thermophoretic is a function of the temperature gradient. The virtual mass is a reaction force exerted on a particle moving through a fluid and will be remarkable when the density of the surrounding fluid is of a similar order of magnitude to the particle density. The Brownian force on the particle is important when the size of the particle is in the submicron range. When the particle is charged or an electric field is applied to the system, electrostatic forces occur. In this study, the acting forces on the particle include the drag force, electrostatic force, and Brownian force. The general equation of the thermophoretic force is a function of ∇T. In this study, there is no temperature difference in the fluid flow, particles, and walls. So, the ∇T is equal to zero. Therefore, the thermophoretic force is zero. Also, the virtual mass is a reaction force exerted on a particle moving through a fluid and will be remarkable when the density of the surrounding fluid is of a similar order of magnitude to the particle density. In this study, the deviation between consideration and neglection of the virtual mass on the particles in two case studies is below 1.0 % in removal efficiency. Also, the reference [40] shows that for a gas-solid two-phase flow, the neglection of the virtual mass is an acceptable approximation. Also, other forces according to air and particle density (related to virtual mass force), particle size and mass (related to gravity force), and lack of temperature gradient (related to thermophoretic force) are neglected in the particle motion [41,42].

The particle motion in a flow is arrived at according to Newton's law as follows [41,43]:

$$m_p\frac{du_p}{dt} = F_D + F_E + F_B \tag{3}$$

$$F_D = m_p \quad \frac{18\mu}{\rho_p d_p^2}\frac{C_D \mathrm{Re}_d}{24}(u - u_p) \tag{4}$$

$$F_B = m_p \quad \sqrt{\frac{216}{\pi}\frac{\mu kT}{C_c \rho^2 d_p^5 \Delta t}} \tag{5}$$

$$F_E = q_p E \tag{6}$$

Where F_D, F_E and F_B are drag force, electrostatic force, and Brownian force, respectively. m_p(kg) is particle mass and u_p(m/s) is particle velocity.

The drag force is calculated by Eq. (4), where d_p(m), ρ_p(kg/m^3), Re_d (-) are particle diameter, particle density, and particle Reynolds number. C_D is the drag coefficient and different models are available to calculate it based on Reynolds number and particle concentration. In this study, the Schiller-Naumann drag [44] correlation showed the best agreement. Brownian force is calculated by Eq. (5), where K is the Boltzmann constant and G is the Gaussian probability density function bounded by − 1 and + 1.

Electrostatic force on a particle is solved by Eq. (6), where q_p(C) is the particle charge and E(N/C) is the electric field. The electric field is solved by the Laplace equation as follows, where V(v) is voltage:

$$E = -\nabla V \tag{7}$$

The particle achieves charge by transferring charge from ions to the particle. The first mechanism for transferring charge to the particle is diffusion charging which is dominant for a particle's diameter smaller than 0.2 μm. In this mechanism, particles are charged by ionic collision due to the thermal motion of the ion. The second mechanism for charging a particle is field charging which is confirmed for particles with a diameter larger than 0.5 μm. Field charging is based on ionic collision affected by an external electric field. In this study, the Lawless model [45], as a combined charging rate model, is used to calculate of charge rate on the particle. In this study, a uniform fiber potential and particle charge distribution are assumed. The field and diffusion charging equations are as follows [1,6,45,46]:

$$\frac{dq_f}{dt} = \pi b N_0 d_p^2 E_0 G\left(1 - \frac{q_e}{d_p^2 E_0 G}\right)^2 \tag{8}$$

$$G = 1 + 2\frac{\varepsilon_p + 1}{\varepsilon_p + 2} \tag{9}$$

$$\frac{dq_d}{dt} = \pi V_{rms} N_0 d_p^2 \quad \exp(-\frac{q_e{}^2}{d_p KT}) \tag{10}$$

Eq. (8) shows the field charging rate, where q_f(C) is the field charging, b (m^2/Vs) the ion mobility, N_0(ion/m^3) is the concentration of ions, E_0 (V/m) is the electric field strength, and ε_p (-) is the relative permittivity of the particle, respectively. Eq. (10) shows the diffusion charging rate where, q_d(C) is diffusion charging, V_{rms}(m/s) is the root-mean-square thermal velocity of the ion, and K (J/K) is Boltzmann constant. By the combination of Eqs. (8), (9), and (10), the field and diffusion charging of the particle is obtained and then the electric field force is computed by Eq. (6). Then the particle moving is calculated by Eq. (3).

2.1.3. Triboelectric nanogenerator

The contact-separation TENG consists of two electrodes with an air gap between them. The electric field around the triboelectric includes three parts; upper dielectric, lower dielectric, and air gaps, so based on Gauss' law [47]:

$$E_{upper} = -\frac{Q}{S\varepsilon_0\varepsilon_{r1}} \tag{11}$$

$$E_{\text{air}} = \frac{-\frac{Q}{S} + \sigma}{\varepsilon_0} \tag{12}$$

$$E_{lower} = -\frac{Q}{S\varepsilon_0\varepsilon_{r2}} \tag{13}$$

Where E (N/C) is the electrical field, Q(C) is induced charge, σ (N/m^2) is surface charge density, S(m^2) is dielectric surface area, ε_r (-) is the relative dielectric constant and ε_0 (C^2/N.m^2) is vacuum permittivity.

The voltage output of the triboelectric nanogenerator is carried out based on Maxwell's theory. The output voltage can be obtained as Eq. (16) [12,48]:

$$V = \int E.dn \tag{14}$$

$$V = E_1 d_1 + E_2 d_2 + E_{air} x \tag{15}$$

$$V = -\frac{Q}{S\varepsilon_0}\left(\frac{d_1}{\varepsilon_{r1}} + \frac{d_2}{\varepsilon_{r2}} + x(t)\right) + \frac{\sigma x(t)}{\varepsilon_0} \tag{16}$$

Where n(-) is the coordinate perpendicular to the surface, d(m) is the dielectric thickness and x(m) is the vertical distance between two electrodes.

In the open circuit (OC) condition, it is assumed that charge transfer, Q, is equal to 0 in Eq. (16), so V_{OC} is equal to:

$$V_{OC} = \frac{\sigma x(t)}{\varepsilon_0} \tag{17}$$

The removal efficiency of the filter is calculated based on the deviation between the entry particle at the inlet and scape particles at the outlet, as Eq. (18):

$$\eta = \frac{m_{p\ \ inlet} - m_{p\ \ outlet}}{m_{p\ \ inlet}} \times 100 \tag{18}$$

By solving Eqs. (1) and (2) the airflow velocity field is obtained. Also, by solving Eqs. (3) to (10), particle motions are calculated. Thereafter, the removal efficiency is calculated by using Eq. (18). The required voltage to reach the best filtration performance can be calculated using the above equations. Then two pairs of triboelectric materials that can produce this voltage are selected. Finally, the open circuit voltage of the TENG is achieved by knowing of tribo-charge of the material by Eq. (17). The boundary condition of each equation is shown in the boundary condition section.

2.2. Geometrical description

The geometrical parameters and adsorption process of the particle are shown in Fig. 1(a). The calculation domain includes a channel with an inlet and outlet. The fibers with a specified design size of the diameter, vertical, and horizontal distance are placed in the middle of the channel. The uncharged particles that are entered the domain are affected by the electrostatic forces. Then the particles are charged and adsorbed to the grounded electrodes.

The geometry of the simulation domain is shown in Fig. 1(b) which gives the detail of the inlet, outlet, fibers, and grounded electrodes positions. In the present study, the fiber diameter, layer thickness (the distance between the first fiber and the last own), and pore size (vertical and horizontal distance between two fibers) are selected near the common face mask [49–54] and given in Table 1.

2.3. Boundary conditions

Constant velocity for the gas flow has been considered as the inlet boundary condition and also the atmospheric pressure is considered as the outlet boundary condition. At the fiber's surface, the no-slip boundary condition is employed for the gas velocity components. The air velocity in the face mask is studied at 2.5 cm/s, 5.0 cm/s, and 7.5 cm/s. Also, the air velocity in industrial air filters is studied at 1.0 cm/s, 2.5 cm/s, and 5.0 cm/s. As well as, symmetry condition is imposed at the grounded electrodes for the airflow. Particles are injected at the inlet and have the same velocity as the airflow. Also, it is assumed that charged particles are adsorbed to grounded electrodes [55,56]. According to the Laplace equation, four boundary conditions are needed to solve an electrostatic domain. Constant voltage is assumed on the fibers surface, inlet, and outlet. Also, the symmetric condition is considered at grounded electrodes.

The performance of the filtration is a measure considered for various particles such as dust airborne and virus particles which have different ranges of diameters and velocity motions. Thus, different ranges of voltage should be applied for different usages. For example, the utilization of low voltages is necessary for smart face masks due to human health and comfort avoiding even small electric shocks. In this study, 0 V,5 V, and 10 V are applied as a smart mask filter, which is widely accepted in human health application monitoring [57]. And the voltage 0 kV,10 kV, and 20 kV are selected as an industrial filter which is consistent with the commonly applied voltage in industrial filters [58]. Furthermore, the particle diameter is selected between 20 nm and 50 μm covering the size of aerosol particles generated during human breathing and industrial dust airborne, which is matched with the common particle size [59,60]. The particle velocity for face mask applications is typically set between 2.5 cm/s and 7.5 cm/s, which corresponds to the airflow velocity during human respiration [61,62]. For industrial applications, a particle velocity range of 1.0 cm/s to 5.0 cm/s is assumed, which is consistent with the airflow velocity in various industrial channels such as clean rooms, HVAC systems, and food processing plants. This low-velocity range is often desired in these industries to minimize turbulence, reduce the spread of airborne particles, and maintain temperature control. The boundary conditions of the electrostatic, airflow, particle trajectory, and also fiber's structure properties are summarized in Table 1 for industrial filter and face mask usage.

2.4. Grid independence

Mesh independence is investigated to keep the computational costs low while ensuring the accuracy of the model. Three different mesh sizes are used in this work and their removal efficiency is compared. In addition, the smallest mesh size has selected enough fine to resolve near-wall regions whit high accuracy. It was observed that there was no significant change in removal efficiency beyond the 23,126 grides. Thus,

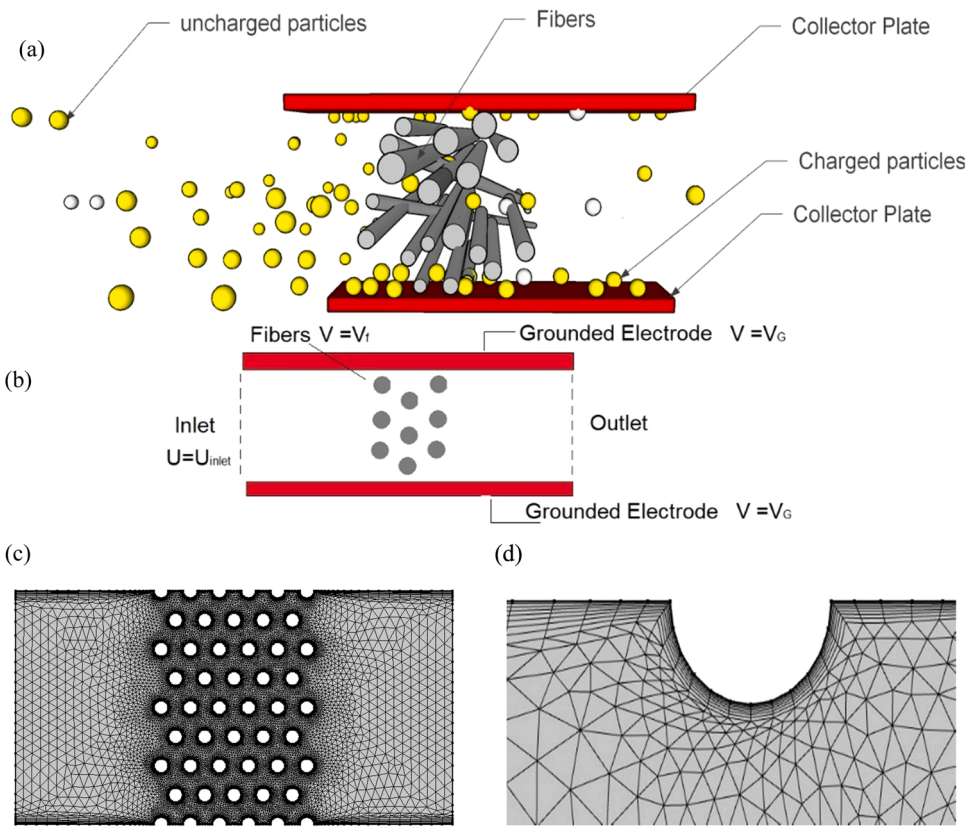

Fig. 1. (a) The schematic diagram of the particle adoption process in the presence of electrostatic force, (b) 2D simulation domain with boundary conditions, (c) the generated mesh of the simulation domain, and (d) finer mesh near the walls and fibers.

Table 1
Simulation design parameters.

Face mask usage			Industrial air filter usage		
Parameter	Unit	Value	Parameter	Unit	Value
Pore size	μm	30	Pore size	μm	30
Fiber's vertical distance	μm	15	Fiber's vertical distance	μm	15
Fiber's horizontal distance	μm	15	Fiber's horizontal distance	μm	15
Filter thickness	μm	300	Filter thickness	μm	300
Fiber diameters	μm	30	Fiber diameters	μm	30
Fiber surface voltage	V	0, 5, 10	Fiber surface voltage	kV	0, 10, 20
Airflow velocity	cm/s	2.5, 5.0, 7.5	Airflow velocity	cm/s	1.0, 2.5, 5.0
Particles size	nm	20–50,000	Particles size	nm	20–50,000

it is chosen as the optimal grid to simulate the domain which is shown in Fig. 1(c,d).

3. Results and discussion

3.1. Model validation

In this study, a mathematical model is developed as a new method and technology for air filters. To reach this goal, the TENG mathematical model is developed and modified for particle motion in the flow that is affected by electrostatic force. To ensure the accuracy of the developed model, all of the physical models are validated separately such as fluid flow, electrostatic, particle motion, removal efficiency, and TENG-produced voltage by reliable reference using two references [25,29]. Also, the TENG- produced voltage is verified by experimental simulation of reference [63].

For validation in order to ensure the accuracy of numerical simulation, the electrostatic forces, airflow fields, and removal efficiency are compared with Choi's [25] work. The reference [25] is selected for model validation as it incorporates both fluid flow and electrostatic contour results. Utilizing this reference could ensure that developed electrostatic and fluid models are accurate and dynamic, as it is able to independently validate both physics. The calculation conditions for verification are as follows: the applied voltage on the fiber surface, inlet, and outlet are 10 V, 9.88 V, and 9.96 V, respectively. Air velocity is 5.0 cm/s. Also, fiber diameters, the vertical and horizontal distances between the two fibers are 30 μm, 60 μm, and 60 μm, respectively.

The comparison between the results of the present study and Choi's [25] work is shown in Fig. 2 for electrostatic and air velocity. As shown in Fig. 2(a,b), the results indicate that the maximum velocity is about 9.87 cm/s near the fiber surface which agrees with the reference [25]. As shown in Fig. 2(c,d), the maximum and minimum electrostatic magnitude in contour is fitted with reference [25]. Furthermore, the efficiency is calculated in the same condition as the reference [25], and the maximum deviation is about 5.0 %. It can be seen that a general agreement is achieved between the reference [25] and this numerical study. Also, the results of the developed model are compared with the reference [29] and shown in Fig. 2(e,f) and Fig. 2(g,h) for fluid flow and particle motion under electrostatic force.

Following validation, the boundary conditions and particle properties are adjusted to meet the requirements of the present study. As particle motion is a transient process, the removal efficiency is calculated for various particle diameters and at different times to ensure its temporal stability. Our findings reveal that the removal efficiency stabilizes within 2.5 s

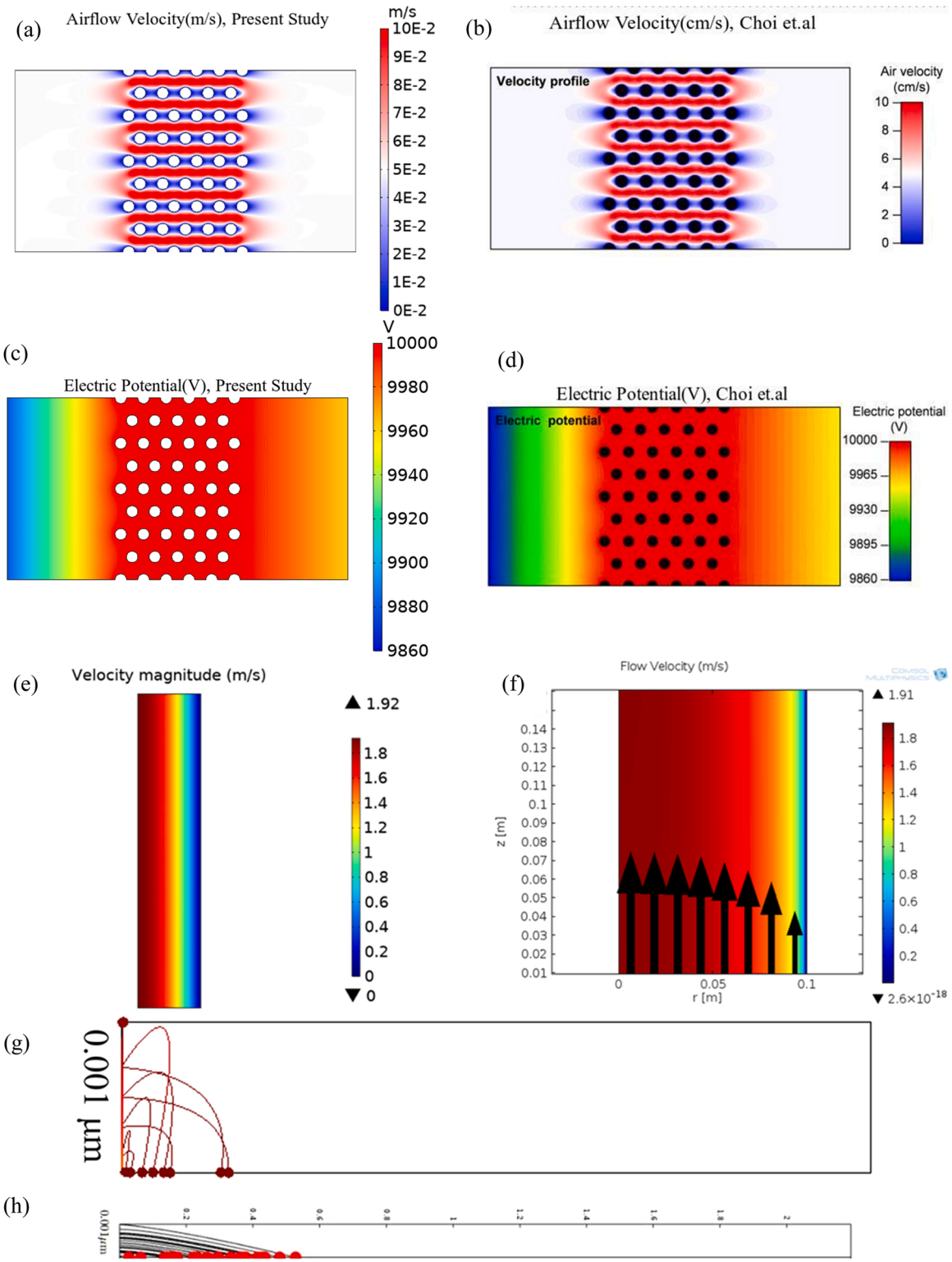

Fig. 2. Model validation. Comparison of airflow velocity of (a) the present model with (b) Choi's [25] work. Comparison of the electric field between (c) present model with (d) Choi's [25] work. Comparison of airflow velocity of (e) the present model with (f) reference [29]. Comparison of the particle adsorption between (g) present model with (h) reference [29].

3.2. The effect of the electrostatic field on removal efficiency

The study investigates the impact of applied voltage on the adhesive force between particles and grounded electrodes. Electric potential contours at 0 kV, 10 kV, and 20 kV applied voltage on the fiber surface are shown in Fig. 3(a), (b), and (c), respectively. The behavior of particles with a radius of 10 nm and a velocity of 2.5 cm/s is analyzed under the applied voltages of 0 kV, 10 kV, and 20 kV. The particle tracking is depicted in Fig. 3(d-f). Based on Fig. 3(d), in absence of the electric field (0 kV), a considerable proportion of particles escape from the domain, leading to an approximate removal efficiency of 20.0 % based on mechanical separation. Conversely based on Fig. 3(e,f), under

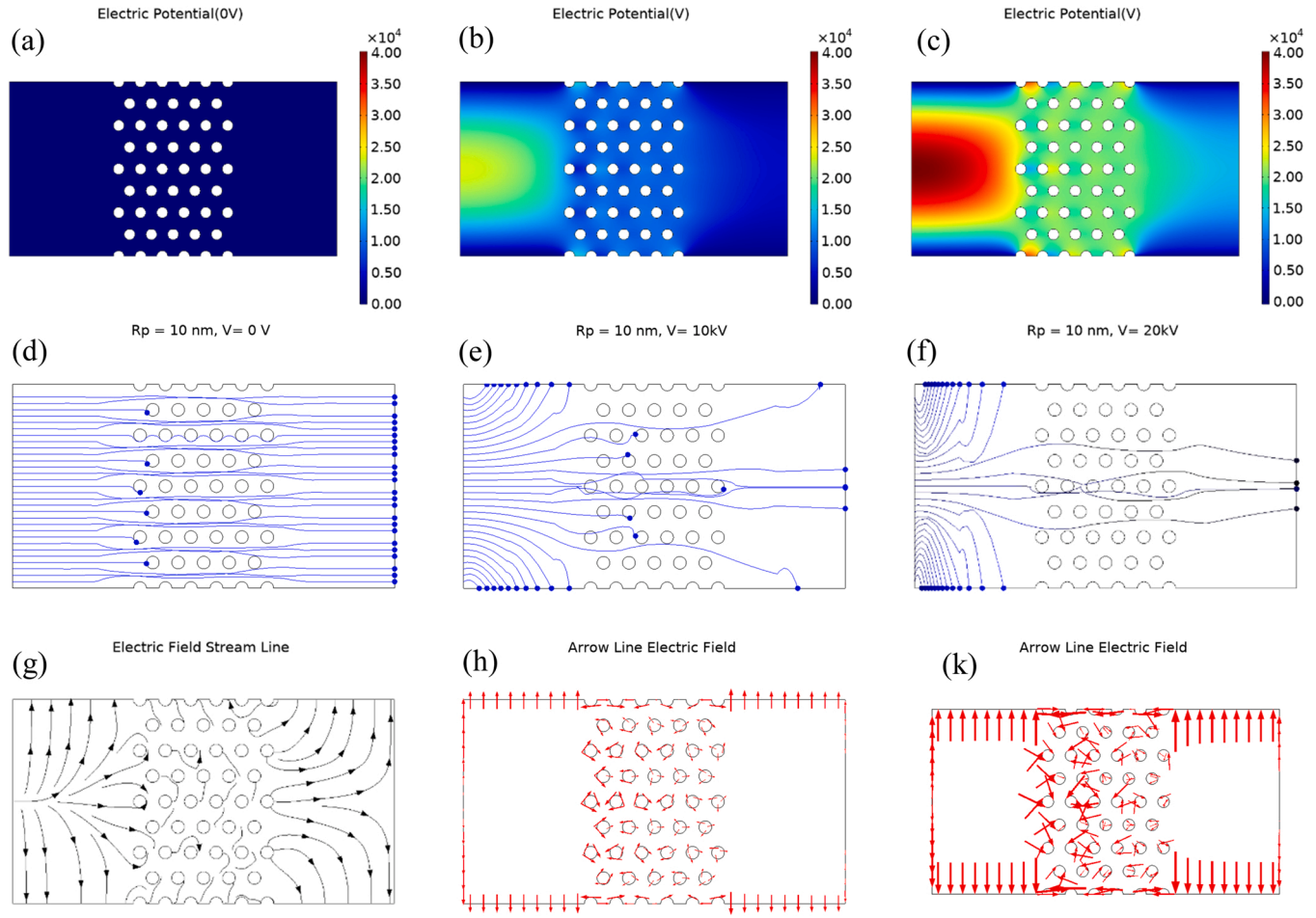

Fig. 3. Impacts of electrostatic forces on the particle removal efficiency: The electric potential contour with different applied voltage on fiber surface: (a) 0 kV, (b) 10 kV, and (c) 20 kV. The particle trajectory under different applied voltages: (d) 0 kV (whit out voltage), (e) 10 kV, and (f) 20 kV, at 10 nm of radius and 2.5 cm/s of airflow velocity. (g) The electric field streamlines under applied voltage on the fiber surface. The electrostatic arrow line and electric field strength under applied voltage: (h) 10 kV, and (k) 20 kV. (k).

the applied voltage of 10 kV and 20 kV on the fiber surface, the charged particles move towards the grounded electrode, resulting in adsorption onto the grounded electrodes and enhanced removal efficiency. A significant increase in the removal efficiency from 20.0 % to 94.0 % is observed with a rise in applied voltage from 0 kV to 20 kV, which represents a five-fold increase compared to the removal efficiency in fibers without electrostatic force. These results demonstrate that as the voltage increases, the particles become more easily adsorbed due to the strengthening of the electric field.

The electrostatic field is generated by potential difference or voltage gradient and indicates the direction of the electric field vector. As depicted in Fig. 3(g), an electrostatic field streamline is entered from the fiber surface to the grounded electrodes. The electric field is presented in Fig. 3(h) and (k), where the length of the arrow indicates the electric field strength. A comparison between Fig. 3(h) and (k) shows that the applied voltage on the fiber surface at 20 kV exhibits a stronger electric field than at 10 kV. So, this is a result of the strong electrostatic forces that drive an increased number of charged particles toward the ground electrodes.

3.3. The effect of airflow velocity on removal efficiency

Fig. 4 illustrates the effect of different airflow velocities, specifically 1.0 cm/s, 2.5 cm/s, and 5.0 cm/s, on particle behavior when the applied voltage is 10 kV and the particle radius is 10 nm. The results show that an increase in airflow velocity leads to more particles exiting the domain

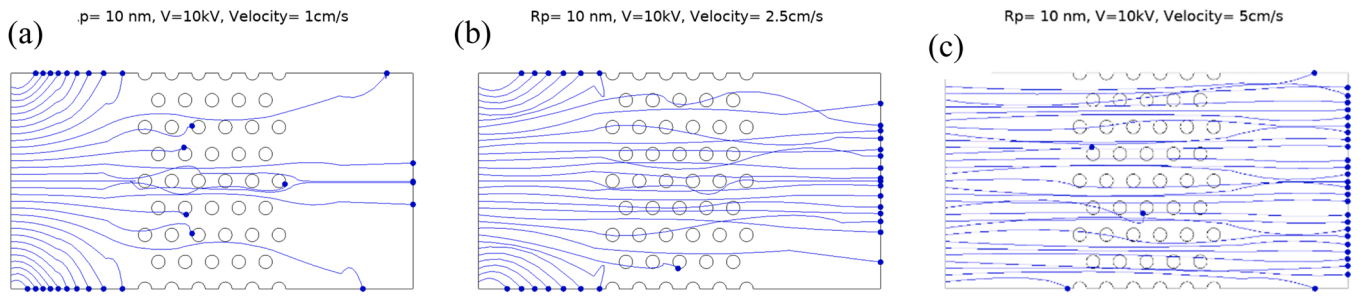

Fig. 4. The particle trajectory under an electric field at different airflow velocities: (a) 1.0 cm/s, (b) 2.5 cm/s, and (c) 5.0 cm/s.

due to the significant influence of gas velocity on particle residence time. Residence time is the average length of time that something moves through a system, which is calculated as the ratio of the volume to the volumetric flow rate. At high velocities, the particle residence time is inadequate for the electric field to effectively act upon the particle. Therefore, as the airflow velocity increases from 1.0 cm/s to 5.0 cm/s, the volumetric flow rate increases 5 times, resulting in a corresponding 5-fold decrease in the residence time. As a result, there is a 70.0 % decrease in removal efficiency, with the efficiency reduced from 86.0 % to 16.0 %. Also, at the radius of 5 μm, the removal efficiency decreases from 99.0 % to 56.0 % when the air velocity increases from 1.0 cm/s to 5.0 cm/s.

3.4. The effect of particles diameter on removal efficiency under the electrostatic field

The impact of particle diameter on particle trajectory under an electrostatic field is depicted in Fig. 5(a-e). The study was conducted at particle radii of 10 nm, 200 nm, 2 μm, 5 μm, and 50 μm under an applied voltage of 10 kV and an airflow velocity of 2.5 cm/s. The results demonstrate that increasing the particle radius from 10 nm to 50 μm improves the removal efficiency from 46.0 % to 94.0 %. Larger particles with more surface area can accumulate a more electric charge, leading to their adsorption on the grounded electrodes, while smaller particles follow the airflow. Additionally, Fig. 5(f) investigates the filter's pressure drop, which is increased from 0.71 Pa to 3.58 Pa as the airflow velocity is increased from 1.0 cm/s to 5.0 cm/s. The Bernoulli equation explains this increase in pressure drop. In other words, based on the

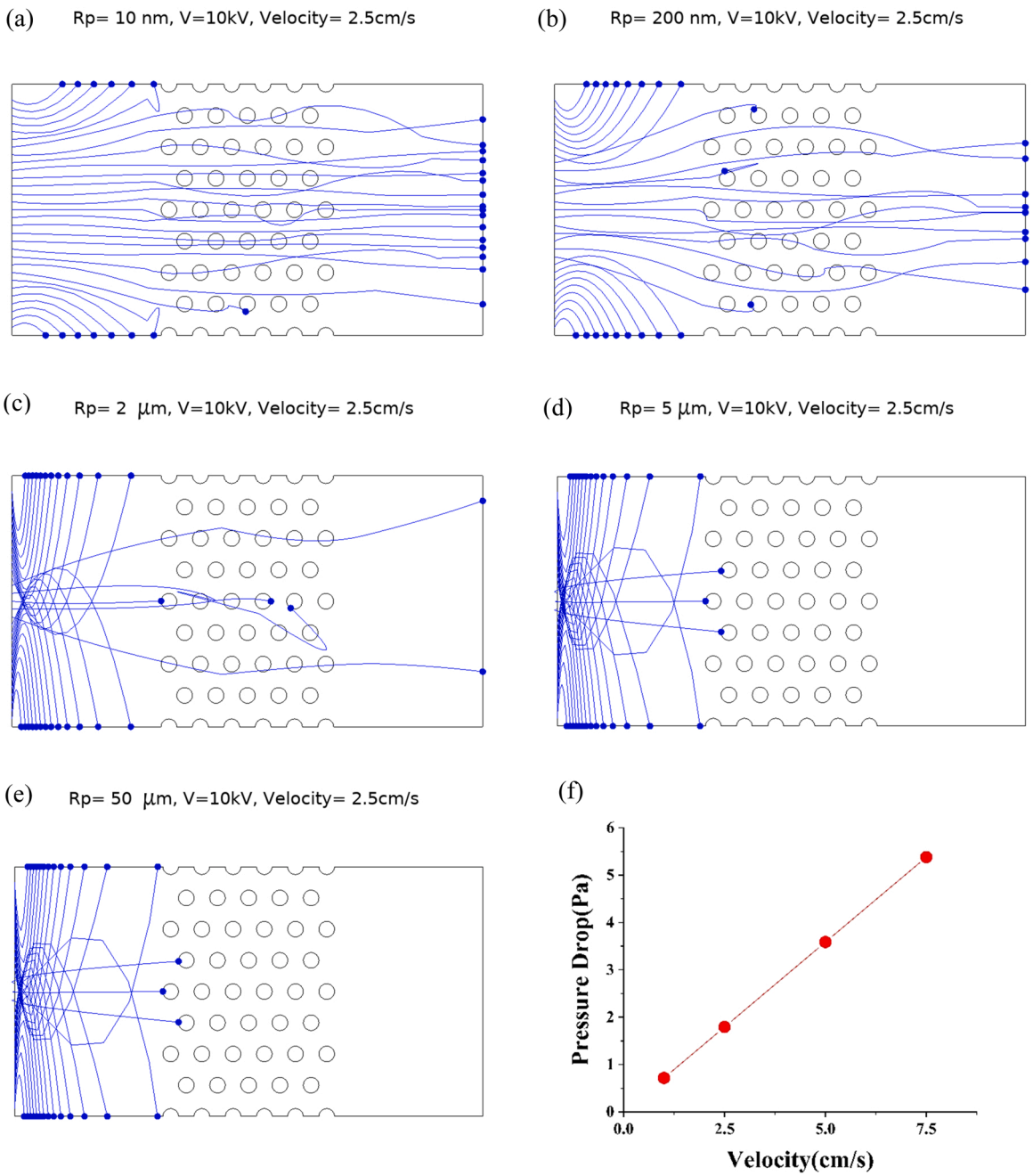

Fig. 5. The particle trajectory under electrostatic field at different particle radii: (a) 10 nm, (b) 200 nm, (c) 2 μm, (d) 5 μm, and (e) 50 μm. (f) The pressure drops at different airflow velocities.

Bernoulli equation, the pressure is decreased in fluid flow regions where the velocity is increased. The pressure drop in porous structures is due to the material's microstructure that can be characterized by various parameters such as pore size, pore shape, and porosity [64]. In common filters, increased packing of fibers can be used for increased filtration which leads to enhanced pressure drops. However, triboelectric forces in TENG absorb small particles reducing the need for compactly packed filters and consequently reducing the pressure drops.

3.5. The optimum voltage range in TENG industrial filter

In industrial air filters, achieving optimal applied voltage is crucial to maintain high efficiency across a range of airflow velocities and particle diameters. To achieve this objective, efficiency is evaluated at various particle diameters and airflow velocities, while applying 0 kV, 10 kV, and 20 kV voltages. In industrial filtration, the removal efficiency of particles in the size range of 20 nm to 10 μm is calculated at a velocity of 2.5 cm/s for 0 kV, 10 kV, and 20 kV, and the results are presented in Fig. 6(a). It is observed that an increase in applied voltage significantly improves the removal efficiency. The efficiency is increased from 23.0 % to 99.0 % with a change in applied voltage from 0 kV to 20 kV, resulting in a four-fold enhancement in removal efficiency. This improvement can be attributed to the strengthening of the electrostatic forces.

The present study aimed to investigate the collection efficiencies of industrial filters under various applied voltages and airflow velocities. Fig. 6(b) displays the removal efficiency of particles calculated at 0 kV, 10 kV, and 20 kV voltage, under 1.0 cm/s, 2.5 cm/s, and 5.0 cm/s airflow velocity. The results show that an increase in airflow velocity leads to a decrease in removal efficiency due to the shorter particle residence time. Specifically, when the airflow velocity is increased from 1.0 cm/s to 5.0 cm/s, the removal efficiency under 10 kV applied voltage decreased from 99.0 % to 86.0 %. However, at 20 kV applied voltage, the removal efficiency remained at approximately 99.0 % under all velocities. The increased removal efficiency can be attributed to the stronger electrostatic forces generated by the higher applied voltage, which allow for more efficient particle collection and removal, even at higher airflow velocities.

Based on the results, the optimal applied voltage for removing particles with diameters ranging from 20 nm to 10 μm is approximately 10–20 kV. These findings suggest that TENG materials that can produce this range of voltage can be used to design industrial air filters capable of removing ultrafine particles ($PM_{0.1}$), fine particles ($PM_{2.5}$), and coarse particles (PM_{10}), covering all dust particles produced by industry.

3.6. The optimum voltage range in the TENG face mask

The optimal applied voltage for face mask filters is a voltage that maintains efficiency at varying airflow velocity and particle diameters. To achieve this goal, efficiency is calculated at different diameters and flow velocities under voltages of 0, 5 V, and 10 V. The removal efficiency in the smart face mask is evaluated based on diameter size ranging from 20 nm to 10 μm under applied voltages of 0 V, 5 V, and 10 V. As shown in Fig. 6(c), the results indicate that an increase applied voltage led to an increase in efficiency. Based on Fig. 6(c), applying a voltage of 5 V to the filter leads to a removal efficiency of 94.0 %. While applying a voltage of 10 V resulted in a removal efficiency of 99.0 % for

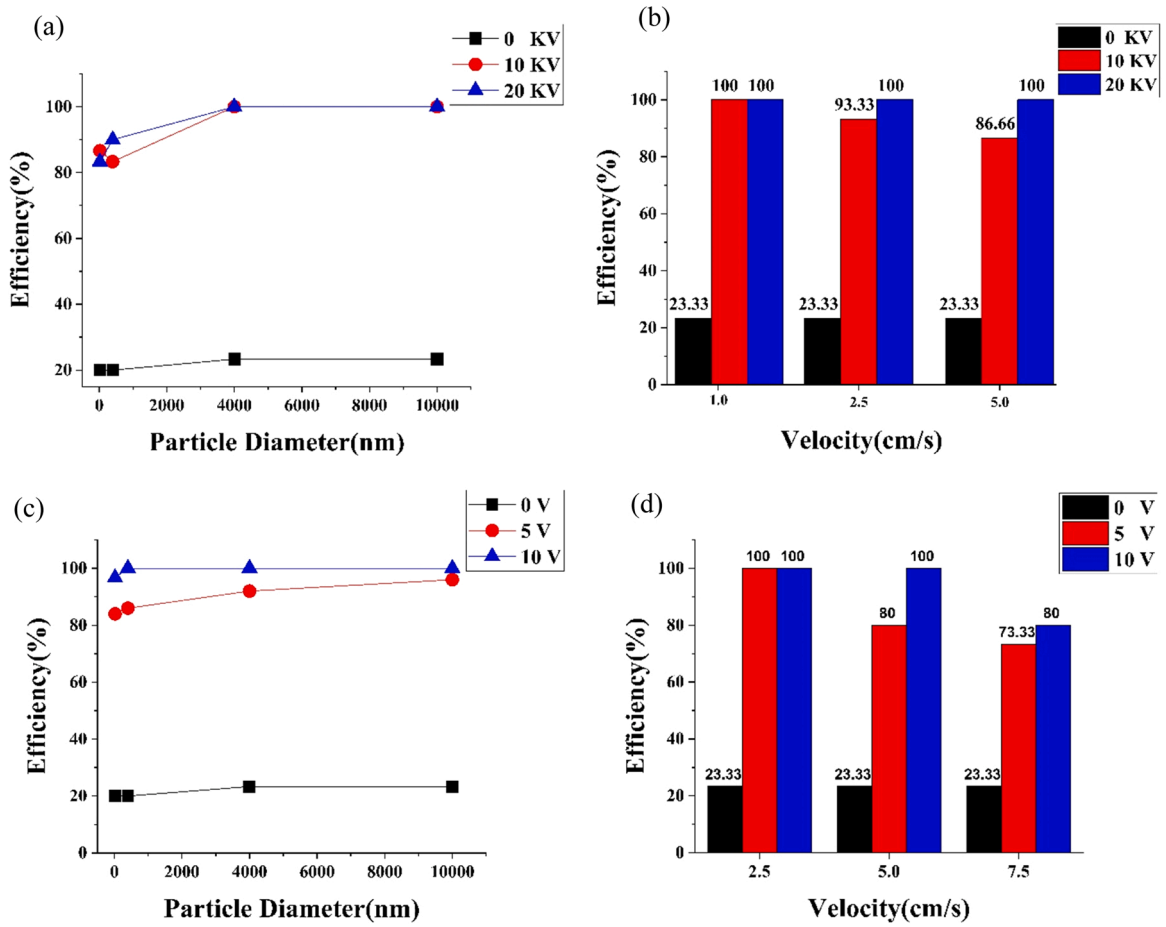

Fig. 6. Removal efficiency to predict the optimum voltage in the face mask and industrial air filter under different airflow velocities, applied voltages, and particle diameters. The removal efficiency of industrial air filters under 0 kV, 10 kV, and 20 kV at (a) different particles size and (b) different airflow velocities. The removal efficiency of the face mask filter under 0 V, 5 V, and 10 V at (c) different particles size and (d) different airflow velocities.

all particulates diameters size from 20 nm to 10 μm which represents a four-fold improvement in comparison to a filter without any applied voltage. The removal efficiencies are calculated at 0, 5 V, and 10 V voltage, under 2.5 cm/s, 5.0 cm/s, and 7.5 cm/s airflow velocity in Fig. 6(d) for face mask usage. When the air velocity is low, the collection efficiency is high and the higher voltage leads to higher efficiency. When the velocity is decreased from 7.5 cm/s to 2.5 cm/s, the efficiency is increased from 80.0 % to 99.0 % at 10 V. This observation can be explained by considering the interplay between the drag force and the electrostatic force. The drag force, which depends on both the air and particle velocity, opposes the motion of the particles, while the electrostatic force, which is proportional to the applied voltage, attracts the particles toward the grounded electrode. Hence, lower airflow velocity reduces the drag force and allows the electrostatic force to dominate, leading to higher collection efficiency.

Results indicate that applying voltage in the range of 5–10 V is optimal for removing particles from 20 nm to 10 μm at different airflow velocities of human breathing in the design of face masks. By applying this voltage range, ultrafine particles ($PM_{0.1}$), fine particles ($PM_{2.5}$), and coarse particles (PM_{10}) can be removed which covers all virus and dust particles size. By using the TENG materials that can produce this range of voltage, it can be designed a TENG smart face mask.

3.7. Design of industrial TENG air filter based on the optimum voltage range

This section discusses the design of self-powered industrial air filters using a contact-separation TENG. Industrial air filters are used in various fields, including the chemical and petrochemical industry, pharmaceutical manufacturing, food and beverage industry, automotive, cement, and mechanical engineering. The qualities of industrial filters should include mechanical and chemical durability, self-cleaning, corrosion resistance, anti-adhesion, and the possibility of regeneration. Therefore, each type of filter requires a specific material for its design. This study employs a range of materials, such as polyester (PES), viscose, polytetrafluoroethylene (PTFE), ethylene chlorotrifluoroethylene (E-CTFE), polyether ether ketone (PEEK), polyvinylidene fluoride (PVDF), polyphenylene sulfide (PPS), PP, polyamide/nylon (PA), PE, and silicon, which are consistent with the common air filter materials [37,65–69].

When filtering hot exhaust gas, it is essential to consider the TENG's

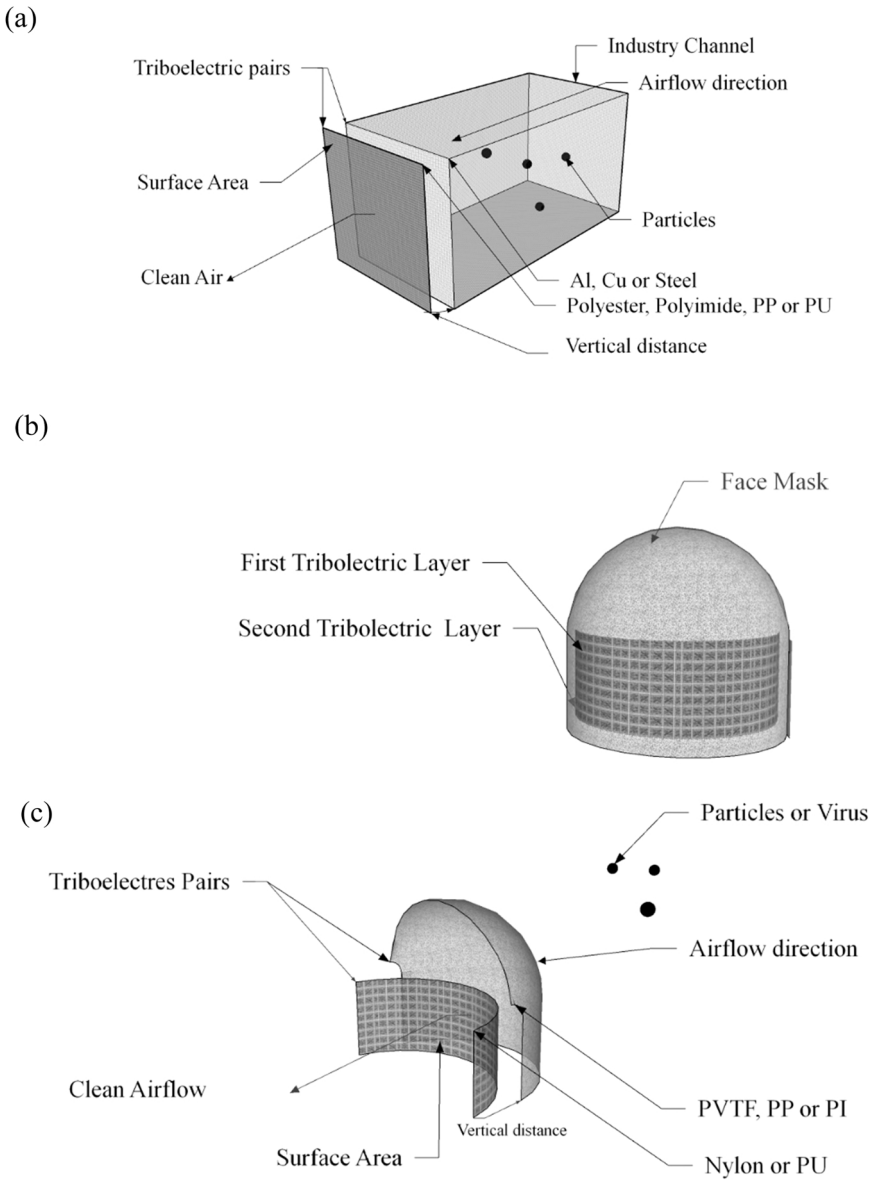

Fig. 7. The design of the contact-separation TENG as a self-powered filter: (a) TENG industrial air filter, and (b,c) TENG face mask.

operating temperature range to select the triboelectric layer. Hence, this study recommends using the silicon family as the triboelectric layer in high-temperature applications, which has a high-temperature yield and is commonly used in such cases [70]. In an air filtration system, the airflow is generated by a fan that pulls or pushes the air. In the presence of this mechanical movement, a contact-separation TENG can be designed to utilize this vibration as a frequency movement source.

Fig. 7(a) displays the parameters and design of the proposed TENG industrial air filter. Polluted airflows enter the inlet channels and pass through the TENG layers, resulting in charged particles that separate from the airflow, allowing clean air to exit the channel. This study suggests that applying a voltage of 10–20 kV produces the most efficient industrial air filters. TENG pairs that generate this voltage are well-suited for air filtration. The recommended design for industrial filters consists of two layers, one of which should be composed of commonly used industrial filter materials such as PES, PVDF, PTFE, or PP. The second electrode could be a metallic mesh like aluminum, copper, or steel. To improve the efficiency of current filters, incorporating a metallic-based mesh is recommended to enhance the triboelectric properties. Specifically, a PE-Cu TENG can be formed where PE serves as the negative layer and Cu as the positive layer. When placed at a vertical distance of approximately 1 mm and moved with the airflow frequency, the voltage produced is around 10 kV. Other suggested triboelectric pairs such as PTE-Cu, PE-Cu, and PLA-Cu can produce voltages of 10–20 kV, where the PE layer and PTE layer have negative triboelectric charges, while the Cu layer has positive triboelectric charges. The pore size, fiber diameter, and layer thickness of the layer in the structure design are the same as those of the common filtration layers [49–54], with dimensions of 30 μm, 30 μm, and 300 μm, respectively. as PTE-Cu, PE-Cu, and PLA-Cu pairs are employed in the design, and the output voltage results are calculated using Eq. (17). The output voltage is calculated per 1 m^2 for industrial use, with a vertical distance of 1 mm between the two layers. In this study, the output voltage is simulated according to Eq. (17) for the proposed TENGs pairs for industrial usage including PTE-Cu, PE-Cu, PU-Cu, and PLA-Cu. Furthermore, the output voltage is calculated for 1 m^2, with a vertical distance of 1 mm between the two layers in a pair with results shown in Fig. 8(a). As shown in Fig. 8 (a), the proposed TENG produced a voltage of about 10–20 kV that is suitable for industrial air filters [58]. The applications of air filters are used in various industries such as mining, renewable power generation, food & beverage packaging, pharmaceuticals, and HVAC. One should note that the duct or channel gas velocity varies significantly for different industrial applications which require accurate modeling for each case. Here, a study has been conducted to investigate the performance of the TENG-based filter at 0.2–0.4 m/s. To investigate the TENG-based filter performance in the HVAC, the airflow velocity is considered about 0.2 m/s, 0.3 m/s, and 0.4 m/s which is consistent with the velocities chosen in [71] and [72]. The removal efficiency for these velocities is shown in Fig. 8(d). The proposed TENG could be utilized as a self-powered air filter or self-powered monitoring sensor, such as gas temperature sensors or pressure sensors, in industrial channels. An industrial air filter based on TENGs could be used for a variety of applications including clean rooms, air conditioning, food processing, and emissions from power plants and automobiles. TENG pairs could be placed at the air ducts and the exhaust channels. Since there is a distance of about 1 mm between the TENG pairs, the pairs contact and separate

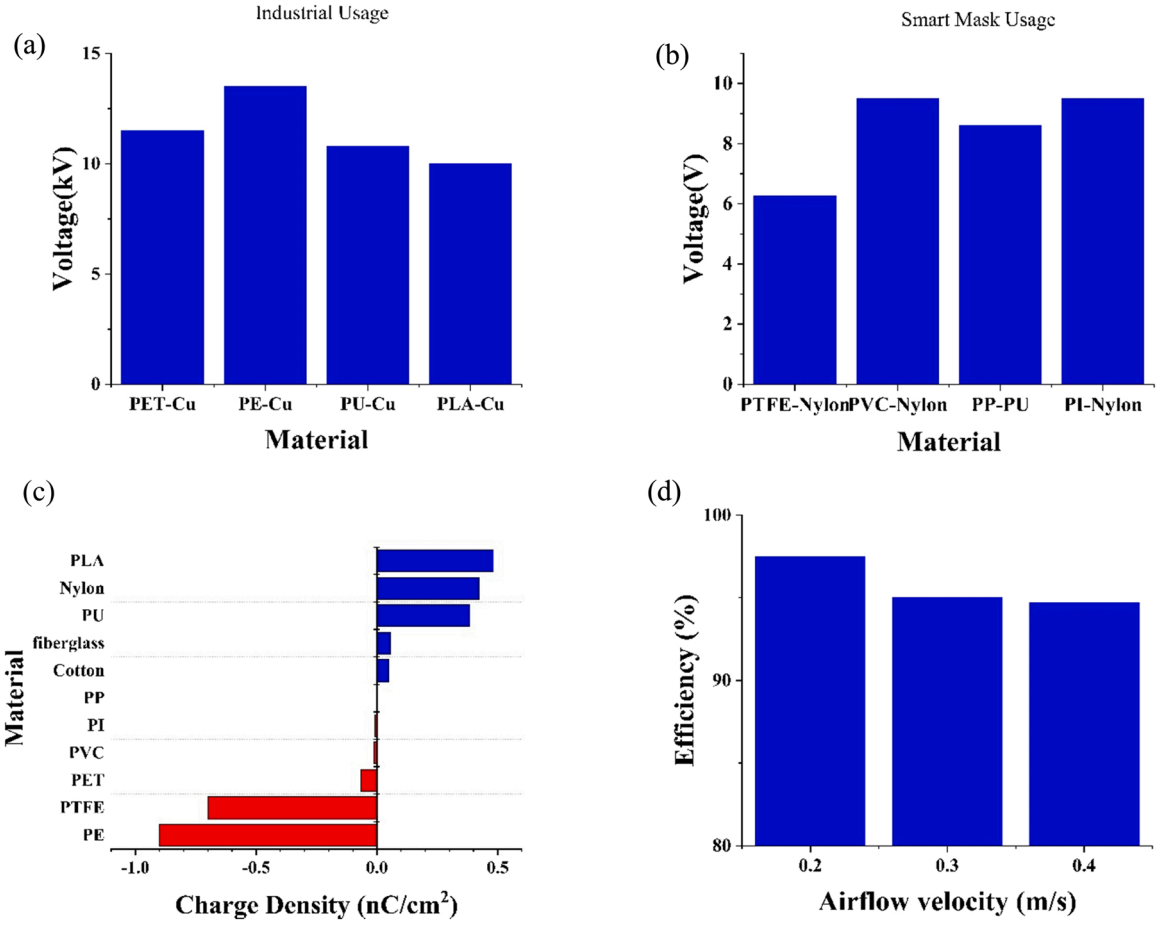

Fig. 8. The generation voltage of the different pairs of the selected triboelectric materials for (a) industrial air filtration, and (b) face mask. (c) The surface charge density of different suggested filters material based on triboelectric series. (d) The removal efficiency in TENG-based filters at 0.2 m/s, 0.3 m/s, and 0.4 m/s airflow velocities.

under the airflow. So, the electrostatic force will be produced in a contact separation mode due to the force obtained by air motion [12]. The produced electrostatic force removes the dust particles.

3.8. Design of TENG face mask based on the optimum voltage range

This section discusses the design of a contact-separation TENG for self-powered smart masks, including the selection of materials, moving source, and design parameters. The selection of appropriate materials is critical in designing TENG face masks. In addition, the applied voltage plays a vital role in the efficiency of the device. Based on the findings of this work, an applied voltage of approximately 5–10 V yields the best results for face masks. Therefore, TENG pairs that can produce this voltage range are ideal for use in face mask design. To design TENG pairs for face masks, a wide range of materials are employed in this study, such as polypropylene, polystyrene, polycarbonate, PE, nylon, polyester, PP, cotton, polyethylene terephthalate (PET), polylactic acid (PLA), polyvinyl chloride, polyamide, polyacrylonitrile (PAN), polyester, polyolefin, thermoplastic, natural cotton, regenerated rayon, cellulose acetate, and PU. These materials are consistent with the common layers of air face masks [25,73–75]. Cu and CuO can be employed as triboelectric materials for the TENG face mask due to their higher degree of antimicrobial activity and hydrophobicity properties [76], which are important properties for masks. In addition, polyester or cotton can be chosen as triboelectric materials for the TENG face mask due to their cloth-like nature, which makes them economical as they can be reused and rewashed multiple times. Furthermore, both polyester and cotton are recommended by the World Health Organization (WHO) due to their hydrophobic properties, which enable them to maintain their efficiency in humid environments when breathing [77]. Therefore, natural triboelectric materials such as Cu, CuO, polyester, and cotton can be chosen for the TENG self-powered face mask. It is important to note that the normal human respiratory rate ranges from 12 to 20 breaths per minute, which is equivalent to a frequency of 0.2–0.33 Hz in the contact-separation mode of the TENG.

Fig. 7(b,c) illustrates a simple design for a TENG filter, where two pairs of triboelectric layers with a vertical distance are placed together and have relative motion through breathing or talking force. This study suggests that an applied voltage ranging from 5 V to 10 V is optimal for achieving the best efficiency in face mask filters. Triboelectric nanogenerator pairs that can produce this voltage range are suitable for TENG face masks. Based on this study, it is recommended that PTFE-Nylon, PVC-Nylon, PP-PU, and PI-Nylon are the best pairs of triboelectric nanogenerators. In these pairs, PVC, PI, and PP are the negative layers, while Nylon and PU act as the positive layers. All of these materials are commonly found in face masks. When placed at a vertical distance of approximately 1 mm and moved with a talking or breathing frequency, the pairs of TENG produce a voltage ranging from 5 V to 10 V. The design values for layer thickness, fiber diameters, and pore size are 300 μm, 30 μm, and 30 μm, respectively, which are in accordance with the typical filter structure [49–54]. Table 2 provides a list of different pairs of materials and their corresponding surface charge densities for designing face masks. Using the total charge density of each pair and the distance between two layers, the voltage generation can be calculated using Eq. (17), which is shown in Fig. 8(b). The surface charge density of the suggested materials for face masks and industrial air filters as positive and negative triboelectric series are also presented in Fig. 8(c). There are various applications that can be applied to TENG-based face masks, including surgery masks, N95s, and cloth masks that only require the use of TENG polymer-based or antibacterial-based pairs as the base materials. The TENG pairs are moved by human breathing as contact- separation mode. So, the produced electrostatic forces are able to remove viruses and dust particles. Humans are protected against viruses and dust particles by using the TENG- face mask. In order to demonstrate the advantages of the TENG-based face mask, a comparison is made between the commercial surgical face mask and the TENG-based mask. The commercial surgical face mask has an efficiency of about 53–75 % but could reach 90 % when another under layer is added to the mask according to [78]. The additional layers would result in increasing the pressure drops in the mask. Also, the filtration efficiency is related to the particle size. The application of the surgical face mask show that the removal efficiency is about 55–85 % and 70–90 % at the 30 and 100 liters in flow rate when particle size is about 300 nm [79]. However, this mask is inefficient in dust-mists and dust-mist-fumes [79]. Based on the concept of triboelectric nanogenerators, the TENG-based mask uses electrostatic forces in addition to the packed fibers. As a consequence, TENG-based masks are expected to remove small particles with less compact or multilayer fibers compared to current commercial surgical masks and N95 masks. So, it leads to a reduction in pressure drops and consequently more comfortable breathing compared to N95 and surgical masks. Another advantage is that the TENG masks' material is as same as the common mask material which is more economical and affordable. Also TENG- masks could use antibacterial material that is helpful in medical applications.

Table 2
Triboelectric material surface charge.

Material	Unit	Triboelectric Charge		Total charge
PTFE-Nylon	(nC/cm^2)	+ 0.7	+0.422	2.78e-1
PVC-Nylon	(nC/cm^2)	-1.17e-5	+0.422	-4.22e-1
PP-PU	(nC/cm^2)	-2.70e-6	+0.385	-3.85e-1
PI-Nylon	(nC/cm^2)	-9.30e-6	+0.422	-4.22e-1

The efficiency of previous TENG-based filter studies is compared with the present model in Table 3.

4. Conclusion

In this study, the application of triboelectric nanogenerator filters has been investigated for improving the removal efficiency of airborne particles and viruses. Specifically, a TENG face mask and an industrial filter have been designed based on the TENG properties, and numerical simulations have been used to predict their optimum voltage range and filtration performance. The results show that applying a 5 V voltage to the filter without any voltage results in a significant increase in the removal efficiency from 23.0 % to 94.0 %, due to the stronger electrostatic forces experienced by the particles. Moreover, the removal efficiency reaches about 99.0 % at 10 V, which is approximately four times higher than that of a filter without any voltage. Furthermore, the effect of airflow velocity on the particle's movement has been investigated. It has been observed that the relaxation time of particles increases as the airflow velocity decreases from 7.5 cm/s to 2.5 cm/s, which allows for more charge to be accumulated on the particles, resulting in an increase in the removal efficiency from 80.0 % to 99.0 %. Based on the results of this study, the optimal voltage range for designing the TENG face mask is between 5 V and 10 V, under 2.5 cm/s to 7.5 cm/s airflow velocity, for eliminating $PM_{0.1}$, $PM_{2.5}$, and PM_{10}. Among the tested triboelectric fabrics, the PI-nylon and PP-PU TENG layers have been found to be the most suitable for the TENG face mask, as they produce a voltage of about 10 V. In addition, the optimal voltage range for designing the industrial air filter has been found to be between 10 kV and 20 kV, under an airflow velocity of 1.0 cm/s to 5.0 cm/s, for eliminating $PM_{0.1}$, $PM_{2.5}$, and PM_{10}. The PE-Cu and PU-Cu TENG layers have been identified as the most suitable for the industrial filter, as they generate a 10 kV voltage. Overall, the results of this study demonstrate that the use of TENG filters is an effective way to enhance the removal efficiency of airborne particles and viruses, without any energy consumption or pressure drop. Based on the results of this work, a wide range of particle sizes, materials, and applied voltages can be investigated to achieve the best filtration efficiency for a special application. The development of self-powered, cost-effective, and pollutant-free TENG face masks and industrial filters, that utilize environmental energy, could have significant

Table 3
Filtration efficiency comparison for various TENG-filter materials and particle sizes.

Material	Particle	Methodology	Efficiency	Reference
Kapton-Copper	SO_2 + dust	Experimental	The maximum adsorption rate was 10–30 %.	[22]
Porous PDMS	PM_{10},$PM_{2.5}$	Experimental	PDMS+ Au NPs had 20 % higher than PDMS/BTO/ fine sucrose and PDMS/ BTO.	[23]
PTFE	$PM_{2.5}$	Experimental	The removal efficiency was about 41 %.	[24]
Kapton+ Al	$PM_{0.3}$,$PM_{0.5}$, $PM_{1.0}$,$PM_{2.5}$, $PM_{5.0}$,PM_{10}	Experimental	In the three-layer mask, the average efficiency was about 89.9 % for $PM_{2.5.}$ And the efficiency was about 90.0 % for particles in the range of 15–550 nm.	[2]
Nylon-polyester, cotton-polyester, PMMA-PVDF, nylon-PVDF, polypropylene-polyester.	Without study	Theory	Without an efficiency report.	[28]
Capable for a wide range of materials for air filters like PTE-Cu, PE-Cu, PU-Cu, and PLA-Cu. Also, for face masks like PTFE-Nylon, PVC-Nylon, PP-PU, and PI-Nylon.	Without bound: wide range of particles that cover the PM and virus size: $PM_{0.1}$ to PM_{10}	Numerical	The removal efficiency is about 94.0–99.0 % for particles in the range of 20 nm to 10 μm.	Present work

implications for public health and safety.

CRediT authorship contribution statement

Masoumeh Karimi-Kisomi: Software, Validation, Writing – original draft. **Sadegh Seddighi:** Supervision, Conceptualization, Software, Writing – review & editing. **Raheleh Mohammadpour:** Supervision, Conceptualization, Writing – review & editing. **Alireza Rezaniakolaei:** Supervision, Writing – review & editing.

Declaration of Competing Interest

The authors declare that they have no known competing financial interests or personal relationships that could have appeared to influence the work reported in this paper.

Data availability

Data will be made available on request.

Acknowledgements

This work is funded by Iran National Science Foundation (INSF) under the contract number 99021716.

References

[1] Ahmadi M., Berkhoff A., de Boer A. Computational fluid dynamics approach to evaluate electrostatic precipitator performance, in: Proceedings of the COMSOL Conference, Rotterdam, 2017.
[2] G. Liu, J. Nie, C. Han, T. Jiang, Z. Yang, Y. Pang, et al., Self-powered electrostatic adsorption face mask based on a triboelectric nanogenerator, ACS Appl. Mater. Interfaces 10 (2018) 7126–7133.
[3] W.H. Organization, Advice on the use of masks in the context of COVID-19: interim guidance, World Health Organ. (2020).
[4] Y. Bai, C.B. Han, C. He, G.Q. Gu, J.H. Nie, J.J. Shao, et al., Washable multilayer triboelectric air filter for efficient particulate matter $PM_{2.5}$ removal, Adv. Funct. Mater. 28 (2018), 1706680.
[5] C. Li, Y. Yin, B. Wang, T. Zhou, J. Wang, J. Luo, et al., Self-powered electrospinning system driven by a triboelectric nanogenerator, ACS Nano 11 (2017) 10439–10445.
[6] D.Y. Choi, S.-H. Jung, D.K. Song, E.J. An, D. Park, T.-O. Kim, et al., Al-coated conductive fibrous filter with low pressure drop for efficient electrostatic capture of ultrafine particulate pollutants, ACS Appl. Mater. Interfaces 9 (2017) 16495–16504.
[7] L. Hou, A. Zhou, X. He, W. Li, Y. Fu, J. Zhang, CFD simulation of the filtration performance of fibrous filter considering fiber electric potential field, Trans. Tianjin Univ. 25 (2019) 437–450.
[8] D.Y. Choi, E.J. An, S.-H. Jung, D.K. Song, Y.S. Oh, H.W. Lee, et al., Al-coated conductive fiber filters for high-efficiency electrostatic filtration: effects of electrical and fiber structural properties, Sci. Rep. 8 (2018) 1–10.
[9] Z. Feng, W. Pan, H. Zhang, X. Cheng, Z. Long, J. Mo, Evaluation of the performance of an electrostatic enhanced air filter (EEAF) by a numerical method, Powder Technol. 327 (2018) 201–214.
[10] E. Tian, F. Xia, J. Wu, Y. Zhang, J. Li, H. Wang, et al., Electrostatic air filtration by multifunctional dielectric heterocaking filters with ultralow pressure drop, ACS Appl. Mater. Interfaces 12 (2020) 29383–29392.
[11] Y. Xu, G. Min, N. Gadegaard, R. Dahiya, D.M. Mulvihill, A unified contact force-dependent model for triboelectric nanogenerators accounting for surface roughness, Nano Energy 76 (2020), 105067.
[12] M. Karimi, S. Seddighi, R. Mohammadpour, Nanostructured versus flat compact electrode for triboelectric nanogenerators at high humidity, Sci. Rep. 11 (2021) 1–15.
[13] M. Duque, G. Murillo, Tapping-actuated triboelectric nanogenerator with surface charge density optimization for human motion energy harvesting, Nanomaterials 12 (2022) 3271.
[14] X. Yin, D. Liu, L. Zhou, X. Li, C. Zhang, P. Cheng, et al., Structure and dimension effects on the performance of layered triboelectric nanogenerators in contact-separation mode, ACS Nano 13 (2018) 698–705.
[15] J. Payen, P. Vroman, M. Lewandowski, A. Perwuelz, S. Calle-Chazelet, D. Thomas, Influence of fiber diameter, fiber combinations and solid volume fraction on air filtration properties in nonwovens, Text. Res. J. 82 (2012) 1948–1959.
[16] M. Zhu, J. Li, J. Yu, Z. Li, B. Ding, Superstable and intrinsically self-healing fibrous membrane with bionic confined protective structure for breathable electronic skin, Angew. Chem. 134 (2022), e202200226.
[17] J. Chen, H. Guo, J. Zheng, Y. Huang, G. Liu, C. Hu, et al., Self-powered triboelectric micro liquid/gas flow sensor for microfluidics, ACS Nano 10 (2016) 8104–8112.
[18] N. Rafiefard, S. Fardindoost, M.K. Kisomi, L. Shooshtari, A. Irajizad, S. Seddighi, et al., High-performance flexible and stretchable self-powered surface engineered PDMS-TiO_2 nanocomposite based humidity sensors driven by triboelectric nanogenerator with full sensing range, Sens. Actuators B Chem. 378 (2023), 133105.
[19] Z. Yan, L. Wang, Y. Xia, R. Qiu, W. Liu, M. Wu, et al., Flexible high-resolution triboelectric sensor array based on patterned laser-induced graphene for self-powered real-time tactile sensing, Adv. Funct. Mater. 31 (2021), 2100709.
[20] M. Zhu, Y. Wang, M. Lou, J. Yu, Z. Li, B. Ding, Bioinspired transparent and antibacterial electronic skin for sensitive tactile sensing, Nano Energy 81 (2021), 105669.
[21] M. Zhu, M. Lou, J. Yu, Z. Li, B. Ding, Energy autonomous hybrid electronic skin with multi-modal sensing capabilities, Nano Energy 78 (2020), 105208.
[22] S. Chen, C. Gao, W. Tang, H. Zhu, Y. Han, Q. Jiang, et al., Self-powered cleaning of air pollution by wind driven triboelectric nanogenerator, Nano Energy 14 (2015) 217–225.
[23] H.-J. Kim, S. Yoo, M.H. Chung, K.-H. Yoo, J. Kim, H. Jeong, Power-free electrostatic collecting film development for purifying indoor air pollution, Nano Energy 65 (2019), 104034.
[24] H.-J. Yoon, D.-H. Kim, W. Seung, U. Khan, T.Y. Kim, T. Kim, et al., 3D-printed biomimetic-villus structure with maximized surface area for triboelectric nanogenerator and dust filter, Nano Energy 63 (2019), 103857.
[25] Y. Cheng, C. Wang, J. Zhong, S. Lin, Y. Xiao, Q. Zhong, et al., Electrospun polyetherimide electret nonwoven for bi-functional smart face mask, Nano Energy 34 (2017) 562–569.

[26] S.R. Lustig, J.J. Biswakarma, D. Rana, S.H. Tilford, W. Hu, M. Su, et al., Effectiveness of common fabrics to block aqueous aerosols of virus-like nanoparticles, ACS Nano 14 (2020) 7651–7658.
[27] G.Q. Gu, C.B. Han, J.J. Tian, T. Jiang, C. He, C.X. Lu, et al., Triboelectric nanogenerator enhanced multilayered antibacterial nanofiber air filters for efficient removal of ultrafine particulate matter, Nano Res. 11 (2018) 4090–4101.
[28] B. Ghatak, S. Banerjee, S.B. Ali, R. Bandyopadhyay, N. Das, D. Mandal, et al., Design of a self-powered smart mask for COVID-19, arXiv Prepr. arXiv 200508305 (2020).
[29] Rubinetti D., Weiss D.A., Egli W. , Electrostatic precipitators–modelling and analytical verification concept, in: Proceedings of the Comsol Conference, University of Applied Sciences Northwestern Switzerland, Windisch, Switzerland, 2015.
[30] P.-O. Persson, J. Peraire, Newton-GMRES preconditioning for discontinuous Galerkin discretizations of the Navier–Stokes equations, SIAM J. Sci. Comput. 30 (2008) 2709–2733.
[31] M. Salehi, A.K. Sleiti, S. Idem, Study to identify computational fluid dynamics models for use in determining HVAC duct fitting loss coefficients, Sci. Technol. Built Environ. 23 (2017) 181–191.
[32] G. Gan, S. Riffat, k-factors for HVAC ducts: numerical and experimental determination, Build. Serv. Eng. Res. Technol. 16 (1995) 133–139.
[33] E. Djunaedy, K. Cheong, Development of a simplified technique of modelling four-way ceiling air supply diffuser, Build. Environ. 37 (2002) 393–403.
[34] Ni P. , A Study on Particle Motion and Deposition Rate: Application in Steel Flows, KTH Royal Institute of Technology, 2015.
[35] H. Xu, S.C. Fu, W.T. Leung, T.W. Lai, C.Y. Chao, Enhancement of submicron particle deposition on a semi-circular surface in turbulent flow, Indoor Built Environ. 29 (2020) 101–116.
[36] S. Adanur, A. Jayswal, Filtration mechanisms and manufacturing methods of face masks: an overview, J. Ind. Text. 51 (2022) 3683S–3717SS.
[37] J. Wang, P. Tronville, Toward standardized test methods to determine the effectiveness of filtration media against airborne nanoparticles, J. Nanopart. Res. 16 (2014) 1–33.
[38] Z. Feng, Z. Long, K. Adamiak, A critical review of models used in numerical simulation of electrostatic precipitators, Inform. Autom. Pomiar. Gospod. Ochr. Środowiska (2016).
[39] M. Zhao, L. Liao, W. Xiao, X. Yu, H. Wang, Q. Wang, et al., Household materials selection for homemade cloth face coverings and their filtration efficiency enhancement with triboelectric charging, Nano Lett. 20 (2020) 5544–5552.
[40] N.I. Kolev, Multiphase flow dynamics 2, Mech. Interact. 4 (2011).
[41] Y.-W. Oh, K.-J. Jeon, A.-I. Jung, Y.-W. Jung, A simulation study on the collection of submicron particles in a unipolar charged fiber, Aerosol Sci. Technol. 36 (2002) 573–582.
[42] H.C. Kim, Numerical analysis of particle transport in low-pressure, low-temperature plasma environment, Part. Aerosol Res. 5 (2009) 123–131.
[43] L. Unger, J.S. Gómez Bonilla, D.A. dos Santos, A. Bück, Particle residence time distribution in a concurrent multiphase flow reactor: experiments and Euler-lagrange simulations, Processes 10 (2022) 996.
[44] F. Yilmaz, M.Y. Gundogdu, Analysis of conventional drag and lift models for multiphase CFD modeling of blood flow, Korea Aust. Rheol. J. 21 (2009) 161–173.
[45] G. Tu, Q. Song, Q. Yao, Experimental and numerical study of particle deposition on perforated plates in a hybrid electrostatic filter precipitator, Powder Technol. 321 (2017) 143–153.
[46] Zhang K., Chen S., Tan L., Xu M., Zhang H., Zhang D. , Study on mechanism and characteristics of particle charging in electrostatic precipitator, IOP Conf. Ser. Mater. Sci. Eng., 2019, 032109.
[47] S. Niu, Z.L. Wang, Theoretical systems of triboelectric nanogenerators, Nano Energy 14 (2015) 161–192.
[48] C. Wu, A.C. Wang, W. Ding, H. Guo, Z.L. Wang, Triboelectric nanogenerator: a foundation of the energy for the new era, Adv. Energy Mater. 9 (2019), 1802906.
[49] S. Choi, H. Jeon, M. Jang, H. Kim, G. Shin, J.M. Koo, et al., Biodegradable, efficient, and breathable multi-use face mask filter, Adv. Sci. 8 (2021), 2003155.
[50] B.B. Neupane, S. Mainali, A. Sharma, B. Giri, Optical microscopic study of surface morphology and filtering efficiency of face masks, PeerJ 7 (2019), e7142.
[51] W. Du, F. Iacoviello, T. Fernandez, R. Loureiro, D.J. Brett, P.R. Shearing, Microstructure analysis and image-based modelling of face masks for COVID-19 virus protection, Commun. Mater. 2 (2021) 1–10.
[52] H.R. Lee, L. Liao, W. Xiao, A. Vailionis, A.J. Ricco, R. White, et al., Three-dimensional analysis of particle distribution on filter layers inside N95 respirators by deep learning, Nano Lett. 21 (2020) 651–657.
[53] Y. Xu, X. Zhang, X. Hao, D. Teng, T. Zhao, Y. Zeng, Micro/nanofibrous nonwovens with high filtration performance and radiative heat dissipation property for personal protective face mask, Chem. Eng. J. 423 (2021), 130175.
[54] D. Das, A. Waychal, On the triboelectrically charged nonwoven electrets for air filtration, J. Electrost. 83 (2016) 73–77.
[55] A. Afshari, L. Ekberg, L. Forejt, J. Mo, S. Rahimi, J. Siegel, et al., Electrostatic precipitators as an indoor air cleaner—a literature review, Sustainability 12 (2020) 8774.
[56] Shah K. , Construction, working, operation and maintenance of electrostatic precipitators (ESPs), Practical Maintenance, 2017.
[57] J. Zhong, Z. Li, M. Takakuwa, D. Inoue, D. Hashizume, Z. Jiang, et al., Smart face mask based on an ultrathin pressure sensor for wireless monitoring of breath conditions, Adv. Mater. 34 (2022), 2107758.
[58] F. Menendez, A. Gomez, F. Voces, V. Garcia, Porcelain insulators in electrostatic precipitator, J. Electrost. 76 (2015) 188–193.
[59] Pedro M. , Filter Considerations in the COVID-19 Era, 2020.
[60] A.-M. Park, S. Khadka, F. Sato, S. Omura, M. Fujita, K. Hashiwaki, et al., Bacterial and fungal isolation from face masks under the COVID-19 pandemic, Sci. Rep. 12 (2022) 1–11.
[61] J.C. Corbin, G.J. Smallwood, I.D. Leroux, J. Norooz Oliaee, F. Liu, T.A. Sipkens, et al., Systematic experimental comparison of particle filtration efficiency test methods for commercial respirators and face masks, Sci. Rep. 11 (2021) 1–16.
[62] H. Souzandeh, K.S. Johnson, Y. Wang, K. Bhamidipaty, W.-H. Zhong, Soy-protein-based nanofabrics for highly efficient and multifunctional air filtration, ACS Appl. Mater. Interfaces 8 (2016) 20023–20031.
[63] M. Karimi, S. Seddighi, R. Mohammadpour, Nanostructured versus flat compact electrode for triboelectric nanogenerators at high humidity, Sci. Rep. 11 (2021) 16191.
[64] W. Zhong, K. Xu, X. Li, Y. Liao, G. Tao, T. Kagawa, Determination of pressure drop for air flow through sintered metal porous media using a modified Ergun equation, Adv. Powder Technol. 27 (2016) 1134–1140.
[65] P. Smith, G. East, R. Brown, D. Wake, Generation of triboelectric charge in textile fibre mixtures, and their use as air filters, J. Electrost. 21 (1988) 81–98.
[66] A. Jaworek, A. Sobczyk, A. Krupa, A. Marchewicz, T. Czech, L. Śliwiński, Hybrid electrostatic filtration systems for fly ash particles emission control. A review, Sep. Purif. Technol. 213 (2019) 283–302.
[67] I. Kim, H. Jeon, D. Kim, J. You, D. Kim, All-in-one cellulose based triboelectric nanogenerator for electronic paper using simple filtration process, Nano Energy 53 (2018) 975–981.
[68] S. Zhu, Y. Xu, C. Huang, X. Jin, Triboelectric effect of polytetrafluoroethylene fibers to improve the filtration performance of air-purified materials, J. Eng. Fibers Fabr. 13 (2018), 155892501801300108.
[69] A. Damokhi, S. Yousefinejad, A. Fakherpour, M. Jahangiri, Improvement of performance and function in respiratory protection equipment using nanomaterials, J. Nanopart. Res. 24 (2022) 1–17.
[70] Y. Zhou, Y. Liu, M. Zhang, Z. Feng, D.-G. Yu, K. Wang, Electrospun nanofiber membranes for air filtration: a review, Nanomaterials 12 (2022) 1077.
[71] C.G. Popovici, HVAC system functionality simulation using ANSYS-Fluent, Energy Procedia 112 (2017) 360–365.
[72] J.A. Siegel, W.W. Nazaroff, Predicting particle deposition on HVAC heat exchangers, Atmos. Environ. 37 (2003) 5587–5596.
[73] T.A. Aragaw, Surgical face masks as a potential source for microplastic pollution in the COVID-19 scenario, Mar. Pollut. Bull. 159 (2020), 111517.
[74] M.Z. Rahman, M.E. Hoque, M.R. Alam, M.A. Rouf, S.I. Khan, H. Xu, et al., Face masks to combat coronavirus (COVID-19)—processing, roles, requirements, efficacy, risk and sustainability, Polymers 14 (2022) 1296.
[75] B. Ghatak, S. Banerjee, S.B. Ali, R. Bandyopadhyay, N. Das, D. Mandal, et al., Design of a self-powered triboelectric face mask, Nano Energy 79 (2021), 105387.
[76] S. Kumar, M. Karmacharya, S.R. Joshi, O. Gulenko, J. Park, G.-H. Kim, et al., Photoactive antiviral face mask with self-sterilization and reusability, Nano Lett. 21 (2020) 337–343.
[77] V. Shruti, F. Pérez-Guevara, I. Elizalde-Martínez, G. Kutralam-Muniasamy, Reusable masks for COVID-19: a missing piece of the microplastic problem during the global health crisis, Mar. Pollut. Bull. 161 (2020), 111777.
[78] A.V. Mueller, M.J. Eden, J.M. Oakes, C. Bellini, L.A. Fernandez, Quantitative method for comparative assessment of particle removal efficiency of fabric masks as alternatives to standard surgical masks for PPE, Matter 3 (2020) 950–962.
[79] S. Rengasamy, A. Miller, B.C. Eimer, R.E. Shaffer, Filtration performance of FDA-cleared surgical masks, J. Int. Soc. Respir. Prot. 26 (2009) 54.

Masoumeh Karimi Kisomi, holds a B.Sc and M.Sc degree in mechanical engineering from Guilan University. Currently, she is a Ph.D. candidate at K. N. Toosi University of Technology. Since November 2022 she joined a research team as a visiting researcher at Aalborg University, Aalborg, Denmark. There, she collaborates with the esteemed Low Power Energy Harvesting & i-Solutions Research Group. Her research interests include energy harvesting, self-powered sensors, fluid mechanics, two-phase flow, and artificial intelligence.

Sadegh Seddighi, obtained his PhD from Chalmers University of Technology in Energy Technology and his M.Sc. from Royal Institute of Technology, Sweden. He is University Vice-Chancellor for Research and Associate Professor of Mechanical Engineering. Sadegh has had various executive positions such as university vice president for International Affairs and has industrial experiences with renowned companies such as Valmet Power Oy and Metso in Finland and Fortum in Sweden and managed various industrial projects in Europe and Asia on energy conversion.

Raheleh Mohammadpour, Associate professor Raheleh Mohammadpour received her B.sc., Msc., and Ph.D. degrees from the Sharif University of Technology with two visiting scholars from Uppsala University and National Chiao Tung University. She has published more than 100 refereed works including papers and conference proceedings. Area of her expertise includes self-powered nanosensors, triboelectric nanogenerators, wearable electronic devices.

Alireza Rezaniakolaei, was born in Babol, Iran in 1983. He received the Ph.D. degree from Aalborg University, Aalborg, Denmark in 2012. Currently, he is Associates Professor of AAU Energy at Aalborg University. He is head of Low Power Energy Harvesting & i-Solutions Research Group with more than 14 years experiences in this field. His current research interests include fluid mechanics, heat transfer, energy harvesting technologies, and integration of these technologies with biomedical, renewable systems, actuators, and sensor applications.